Automated segmentation of middle hepatic vein in non-contrast X-ray CT images based on an atlas-driven approach

Teruhiko Kitagawa*[a], Xiangrong Zhou[a], Takeshi Hara[a], Hiroshi Fujita[a],
Ryujiro Yokoyama[b], Hiroshi Kondo[c], Masayuki Kanematsu[b], Hiroaki Hoshi[d]
[a] Department of Intelligent Image Information, Division of Regeneration and Advanced Medical Sciences, Graduate School of Medicine, Gifu University, 1-1 Yanagido, Gifu-shi, Gifu, Japan 501-1194
[b] Department of Radiology Services, Gifu University School of Medicine, Gifu University, 1-1 Yanagido, Gifu-shi, Gifu, Japan 501-1194
[c] Department of Radiology, Gifu University Hospital, 1-1 Yanagido, Gifu-shi, Gifu, Japan 501-1194
[d] Department of Radiology, Division of Tumor Control, Graduate School of Medicine, Gifu University Yanagido, Gifu-shi, Gifu, Japan 501-1194

ABSTRACT

In order to support the diagnosis of hepatic diseases, understanding the anatomical structures of hepatic lobes and hepatic vessels is necessary. Although viewing and understanding the hepatic vessels in contrast media-enhanced CT images is easy, the observation of the hepatic vessels in non-contrast X-ray CT images that are widely used for the screening purpose is difficult. We are developing a computer-aided diagnosis (CAD) system to support the liver diagnosis based on non-contrast X-ray CT images. This paper proposes a new approach to segment the middle hepatic vein (MHV), a key structure (landmark) for separating the liver region into left and right lobes. Extraction and classification of hepatic vessels are difficult in non-contrast X-ray CT images because the contrast between hepatic vessels and other liver tissues is low. Our approach uses an atlas-driven method by the following three stages. (1) Construction of liver atlases of left and right hepatic lobes using a learning datasets. (2) Fully-automated enhancement and extraction of hepatic vessels in liver regions. (3) Extraction of MHV based on the results of (1) and (2). The proposed approach was applied to 22 normal liver cases of non-contrast X-ray CT images. The preliminary results show that the proposed approach achieves the success in 14 cases for MHV extraction.

Keywords: non-contrast X-ray CT images, liver atlas, atlas-driven segmentation method, middle hepatic vessel, computer aided diagnosis (CAD) system

1. INTRODUCTION

The latest multi-slice X-ray CT scanners generate a large number of slices to construct a volumetric CT images covering a wide volume of human body in a very short time. Although such a volumetric CT image can provide detailed information of human internal organs, the interpretations need a lot of time and energy. Therefore, computer-aided diagnosis (CAD) systems, which can support the multi-lesion interpretations for multi-organs in CT images, are desirable. Such CAD system can increase the lesion detection accuracy of radiologist and decrease the interpretation burden. It is necessary for CAD system to recognize and to segment the anatomical human body structures automatically. Liver region is one of the most important diagnosis targets in abdominal organs for CAD system. Lesion detection and surgery planning of the liver always require CAD system to extract the liver region first and recognize the hepatic vessel trees in CT images.

The liver regions are further separated into Couinaud classification. This classification is important for radiologist to identify the location of lesion inside liver region and decide a surgery planning. The Couinaud classification divides the liver region into eight independent segments (s1-s8), and each segment has its own vessel tree structures (hepatic vein and portal vein: PV) and surrounding organs (e.g., inferior vena cava: IVC, etc.).

* kitagawa@fjt.info.gifu-u.ac.jp

Medical Imaging 2008: Image Processing, edited by Joseph M. Reinhardt, Josien P. W. Pluim,
Proc. of SPIE Vol. 6914, 69144E, (2008)
1605-7422/08/$18 · doi: 10.1117/12.771612

In Couinaud classification, the plane defined by the middle hepatic vein (MHV) and IVC subdivide the liver region into the right (s1-s4) and left (s5-s8) lobes. So, the rule to identify the right and left lobectomy is to find the plane of the MHV and IVC.

Many research works were presented for liver segmentation and hepatic vessel recognition based on contrast-media enhanced or multi-phase abdominal CT images that are routinely used for lesion screening in clinical medicine.[1-6] However, non-contrast CT images are usually scanned before the generation of the contrast- media enhanced CT images as the basic information. So that, automated segmentation and recognition of hepatic vessels in non-contrast CT images are a basic requirement for liver CAD system. In the previous study, we developed a contrast enhancement method for segmenting the hepatic vessels in non-contrast CT images.[7] However, the further improvement for fully-automated recognition of hepatic vessels was required. The hepatic vessel regions have a lower CT number compared to other liver tissues in non-contrast CT images, and the difference in CT number is very small. Therefore, it is difficult to segment the hepatic vessels simply based on CT number.

In our previous work, we proposed an automated approach for liver region segmentation in non-contrast X-ray CT images using probabilistic liver atlas and confirmed the efficiency and accuracy of the method based on a large database.[8-10] In this paper, we propose an atlas-driven approach to extract IVC and MHV regions in non-contrast X-ray CT images as the preparation of analysis of hepatic lobe recognition. In the following sections, we first describe the outline of hepatic vessel extraction and show the details of our approach in Section 2. Experimental results and discussions are presented in Section 3 and 4, respectively. A conclusion is given in Section 5.

2. METHODS

The proposed approach includes two parts, one is the atlas construction using a learning dataset, and the other is MHV segmentation process based on the constructed atlas. The flowcharts of our proposed method are shown in Fig.1 and Fig.2. Fig.1 shows a construction method of hepatic lobe and IVC atlas (2.1), and Fig.2 illustrates a segmentation method of MHV (**2.2-2.4**). The details of each processing step are described as follows:

2.1. Construction of right and left hepatic lobe atlases and IVC atlas

2.1.1 Extraction of liver and IVC region and separating into right and left hepatic lobes

The learning set includes twenty-two liver regions and IVC regions that were extracted using an extraction method

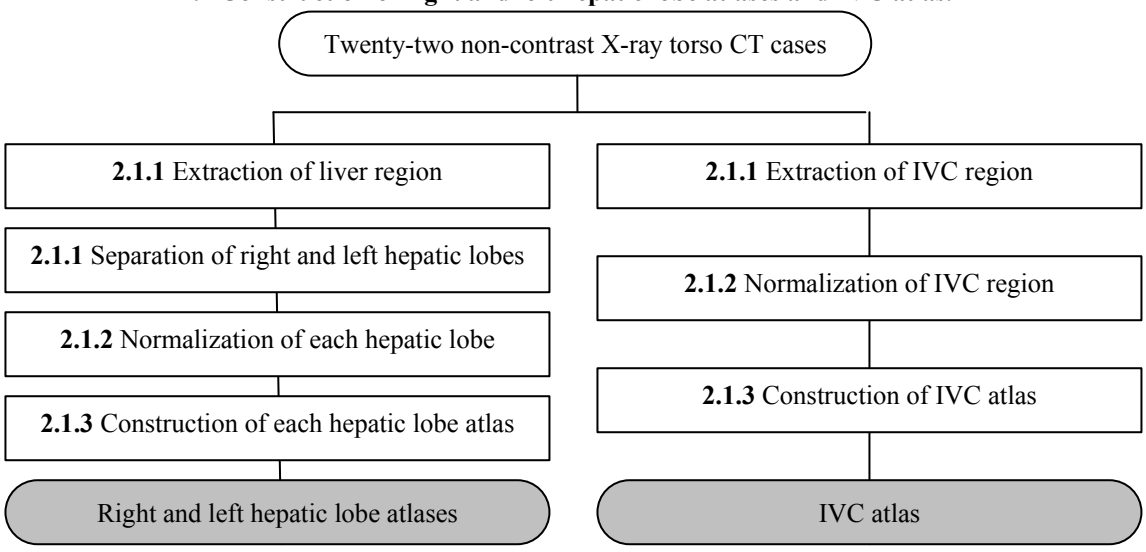

Fig.1 Flowchart of construction method of right and left hepatic lobe atlases and IVC atlas.

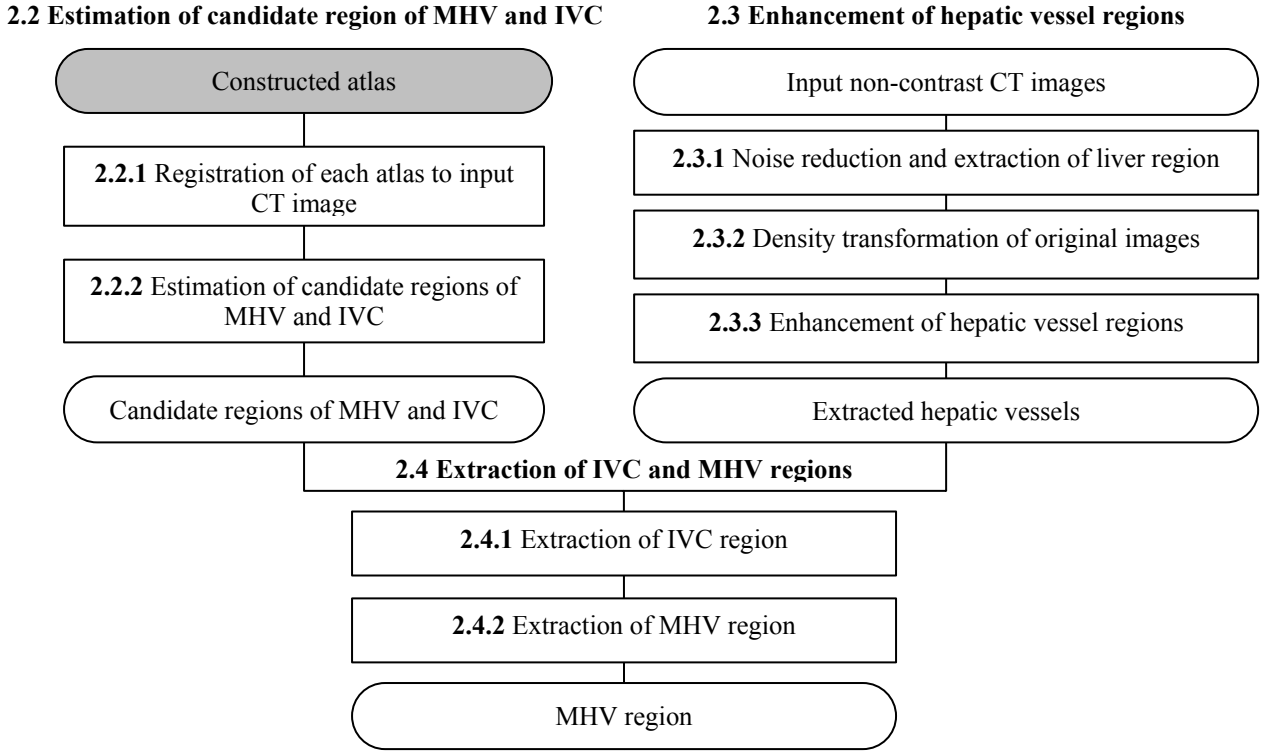

Fig.2 Flowchart of extraction method of MHV region using constructed atlas from input CT images.

based on density distribution, and the liver region was further separated into left and right hepatic lobes manually in non-contrast X-ray CT images [Fig.3 (a)]. These hepatic lobes and IVC regions were defined as "left hepatic lobe gold standard", "right hepatic gold standard" and "IVC gold standard", respectively, and determined based on the decision and interpretations of a radiologist. These gold standards were used to evaluate the extraction result of MHV by the proposed method. Figs.3 (b) and (c) show an example of gold standards of each hepatic lobe (blue: right lobe, red: left lobe and green: IVC).

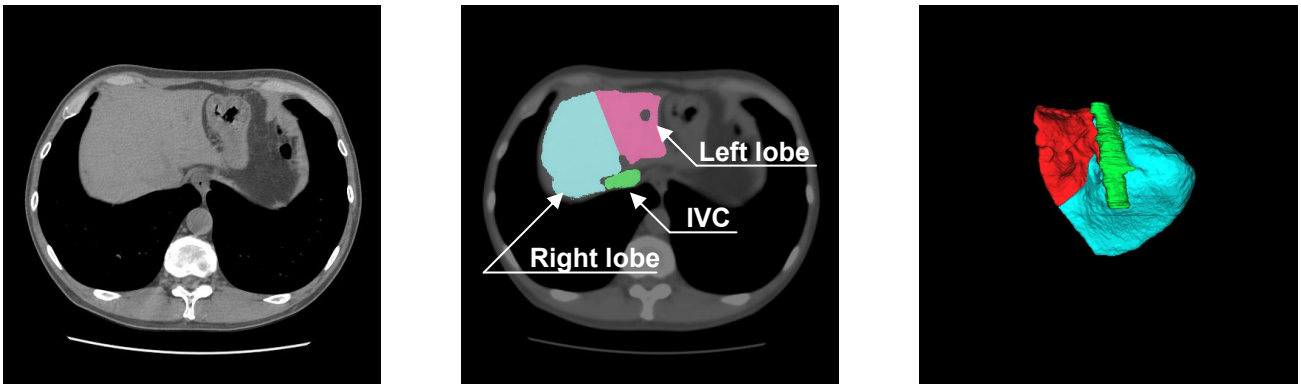

(a) (b) (c)

Fig.3 A result of each region segmented manually. (a) An axial slice of non-contrast X-ray CT image (a part of abdomen), (b) segmented each tissue (blue: right hepatic lobe, red: left hepatic lobe and green: IVC: Inferior vena cava) region segmented manually from (a), and (c) 3D image of (b).

2.1.2 Normalization of locations of hepatic lobes and IVC

The location of each hepatic lobe and IVC gold standards were normalized using a method[8-10] proposed by our research group. This method used information of human body structures (diaphragm,[11] bone structures and skin[12]) as the reference and arrange the locations of the hepatic lobe and IVC in different CT images to a same coordinate space using TPS deformation algorithm.[13] Fig.4 and Fig.3 (c) show an example of the normalized hepatic lobes and IVC region in a CT case.

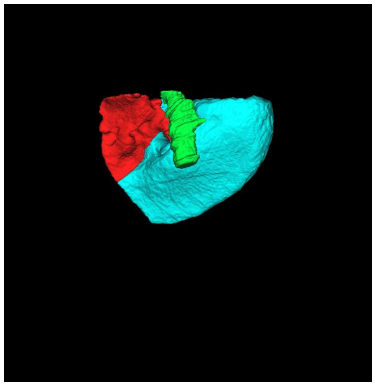

Fig.4 A result of normalized liver region and IVC region using TPS deformation (3D image, blue: right hepatic lobe, red: left hepatic lobe and green: IVC region).

2.1.3 Construction of the atlases hepatic lobes and IVC

Right and left hepatic lobe atlases P_{atlas} were constructed by a spatial voting process based on the normalized 22 right and left hepatic lobes respectively by the following equation.

$$P_{atlas}(x,y,z)=\sum_{i=1}^{N}\frac{I_i(x,y,z)}{N}, \qquad (1)$$

where N was number of cases used for construction of atlas, and $I_i(x, y, z)$ was a function which return 1 when a hepatic lobes and IVC region exists at (x, y, z) in case i. We defined as right hepatic lobe atlas: P_{right}, left hepatic lobe atlas: P_{left} and IVC atlas P_{IVC}, corresponding to each target region respectively. And Fig.5 shows constructed each atlas [(a) P_{right}, (b) P_{left}, and (c) P_{IVC}].

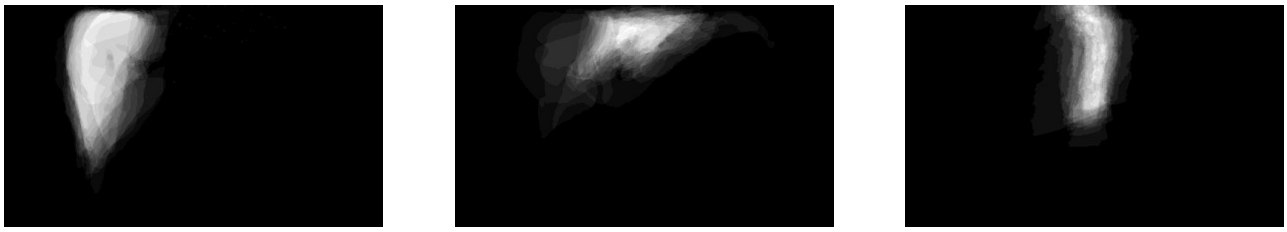

(a) (b) (c)

Fig.5 The constructed probabilistic atlases of (a) right hepatic lobe: P_{Right}, (b) left hepatic lobes: P_{left} and (c) IVC: P_{IVC} using 22 normalized cases.

2.2 Estimation of candidate regions of MHV and IVC

2.2.1 Registration of each hepatic lobe atlas

Constructed atlases for each hepatic lobe and IVC were registered with an input CT case by registering the related anatomical structures of the atlas and input CT case and deforming such atlas to adapt the individual difference of the liver locations based on a TPS deformation algorithm. Deformed atlases were defined as "likelihood image of right hepatic lobe: L_{right}", "likelihood image of left hepatic lobe: L_{left}" and "likelihood image of IVC: L_{IVC}", respectively.

2.2.2 Estimation of candidate region of MHV and IVC

Due to the anatomical knowledge, the MHV is located in the plane which separates the left and right lobe. So that, we estimate the range (a candidate region) which includes MHV region using L_{right} and L_{left}. We defined "candidate region of MHV: $R_{MHV}(x,y,z)$" by following equation (2).

$$R_{MHV}(x,y,z) = \begin{cases} 1 & if\ (L_{right}(\mathrm{x},\mathrm{y},\mathrm{z}) > 0 \cap L_{left}(x,y,z)) > 0 \\ 0 & else \end{cases}, \quad (2)$$

And "candidate region of IVC: $R_{IVC}(x,y,z)$" by equation (3).

$$R_{IVC}(x,y,z) = \begin{cases} 1 & if\ \ (L_{IVC}(\mathrm{x},\mathrm{y},\mathrm{z}) > 0) \\ 0 & else \end{cases}, \quad (3)$$

2.3 Enhancement of hepatic vessel regions

2.3.1 Noise reduction and extraction of liver region

A Gaussian filter was performed to reduce the image noise in input CT images, and then the liver region was extracted from the CT images using an atlas-driven approach that was developed in our previous study. [8-10]

2.3.2 Histogram transformation of input CT images

Because the hepatic vessel regions in non-contrast CT images have a lower CT number comparing with the other liver tissues, a part of hepatic vessel regions can be extracted firstly using a p-tile method based on the CT number distributions. We assumed that CT numbers of hepatic vessel regions can be approximated as a normal distribution, so that the mean value μ and standard deviation σ of CT number in hepatic vessels can be estimated from the CT numbers in the part of hepatic vessel regions that were extracted in the previous step. An enhanced image $L_{density}$ was generated to show the appearance of hepatic vessel by a histogram transformation of input CT image $I(x,y,z)$ using the following equation.

$$L_{density}(x,y,z) = C\exp\left\{-\frac{(I(x,y,z)-\mu)^2}{2\sigma^2}\right\}, \quad (4)$$

Here, C is a non-zero constant value.

2.3.3 Enhancement of hepatic vessel regions

Hepatic vessel regions pre-enhanced in **2.3.2** may include many false positive regions caused by the image noise. We have assumed that the shape of hepatic vessels was similar to a line or cylinder, so a method that can extract the feature of line or cylinder components may be useful for hepatic vessel enhancement. We employed a line-enhancement method[14] based on Hessian matrix on $L_{density}$, and generated a likelihood image L_{vessel}.[7]

2.4 Extraction of IVC and MHV regions

2.4.1 Extraction of IVC

The location of IVC was estimated using R_{IVC} and CT number distribution. Generally, CT number distribution range of IVC was assumed from water (0 [H.U.]) to mean CT number of normal hepatic parenchyma μ_{liver}. μ_{liver} was estimated using histogram of extracted liver region in 2.3.1. We defined the regions that satisfy the following two conditions as IVC.

(a) $R_{IVC}(x,y,z) > 0$.

(b) $0 < I(x,y,z) < \mu_{liver}$.

2.4.2 Extraction of MHV

The location of MHV was estimated using R_{MHV} , L_{vessel} and feature of anatomical structure that part of hepatic vein which originates from IVC. So, MHV region was extracted by selecting the regions that satisfy the following three conditions.

(a) $R_{MHV}(x,y,z) > 0$.

(b) (Maximal number of L_{vessel}) / 3 < $L_{vessel}(x,y,z)$.

(c) Contacting with the IVC.

3. EXPERIMENTS

The proposed method was applied to 22 patient cases of non-contrast X-ray CT images. All patient cases were scanned with a common protocol (120kV/ auto mA) by a multi-slice CT scanner (LightSpeed Ultra of GE Healthcare). These CT images covered the whole human torso area with about 1000 slices, isotopic spatial resolution of about 0.6 (mm) and density (CT number) resolution of 12 bits.

Fig.6 shows examples of likelihood images L_{right} [(a)], L_{left} [(b)], and L_{IVC} [(c)] which registered each atlas, P_{right}, P_{left}, and P_{IVC} to input CT images, respectively. It was found that high likelihood value exists each target structure.

Fig.7 indicates example of R_{MHV} (bright area inside liver region) estimated in 2.2 using Figs.6 (a) and (b). True MHV region exists inside white circle, so this estimation result was accurate.

Fig.8 (a) shows an example of noise reduced input CT image using Gaussian filter. Fig.8 (b) is an enhanced image of Fig.8 (a) using Gaussian window function. In this image, prime vessel regions inside liver region were enhanced, but thin hepatic vessel regions were not enhanced. A slice of enhanced image and MIP image (axial direction) using line enhancement filter, applied to Fig.8 (b) image inside liver region, are shown in Figs.8(c) and (d), respectively. In this image, it was confirmed not only prime hepatic vessel regions but also thin vessel regions which were not enhanced in Fig.8 (b).

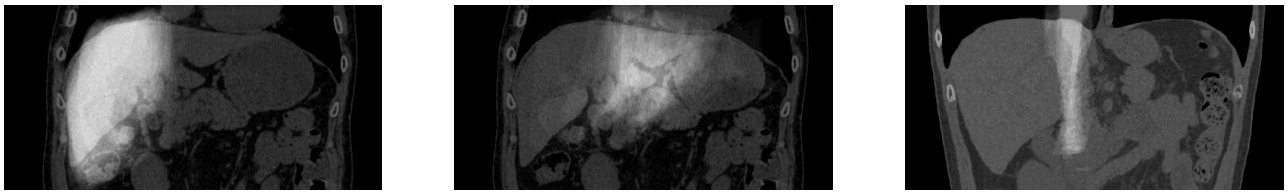

(a) (b) (c)

Fig.6 The constructed likelihood images of (a) right hepatic lobe: L_{right}, (b) left hepatic lobe: L_{left}, and (c) IVC: L_{IVC} using probabilistic atlases.

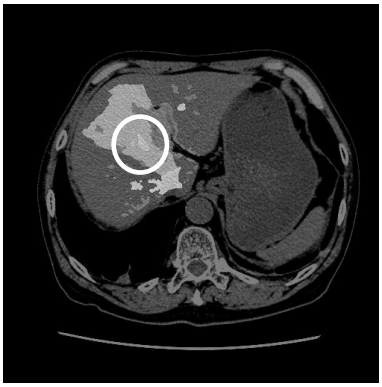

Fig.7 An example of estimated R_{MHV} using L_{right} and L_{left}.(white circle inside : true MHV region).

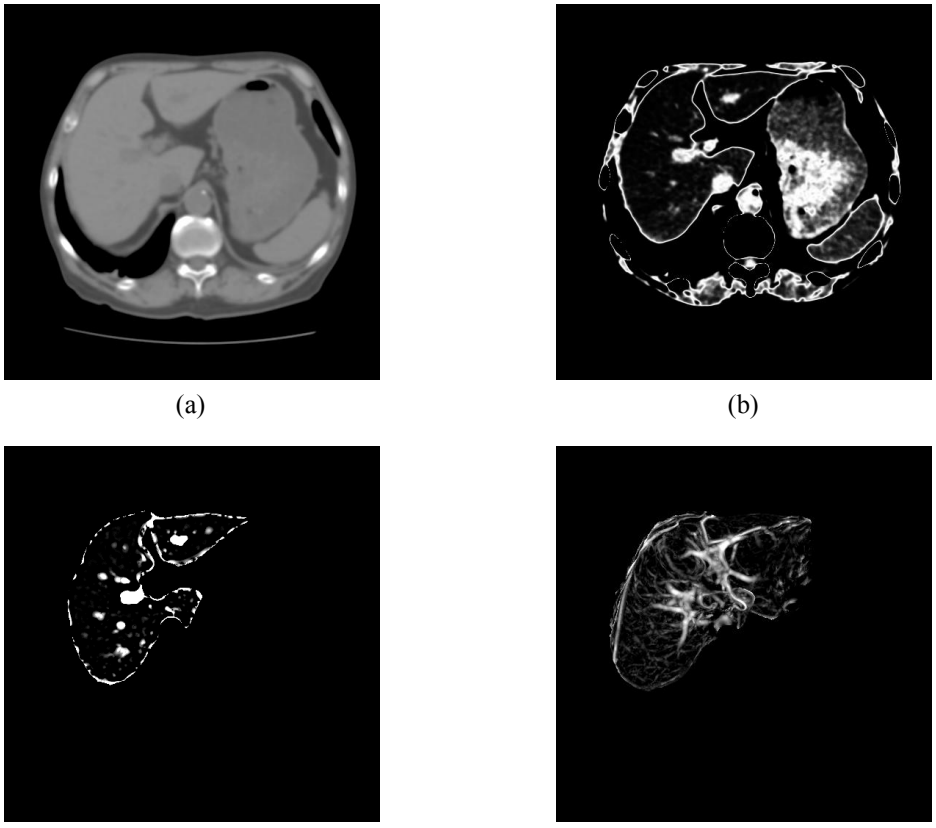

(a) (b)

(c) (d)

Fig.8 Enhancement of hepatic vessels. (a) A result of noise reduced input CT image using Gaussian filter, (b) enhanced (a) image using Gaussian window function, (c) enhanced (b) image using line enhancement filter (inside liver region), and (d) MIP image of (c) (axial direction).

4. RESULTS AND DISCUSSIONS

We applied our method to 22 non-contrast X-ray CT images. All the cases were normal liver cases. The extraction results (MHV) were evaluated by a coincidence ratio between the extracted result and corresponding gold standard of

MHV. We regarded the case that has a coincidence ratio more than 0.30 as the successful case. The results showed that hepatic vessels extracted using our proposed method had a mean coincidence ratio of 0.374 and the coincidence ratio in 63.6% (14/22) cases was larger than 0.30.

Some examples of the results are shown in Fig.9 (3D images, white: over extraction region, light gray: overlapping region between MHV gold standard and extracted region in each CT case). Figs.9 (a) and (b) are examples of successful cases to extract MHV region. On the other hand, Figs.9 (c) and (d) are unsuccessful cases which have over extracted

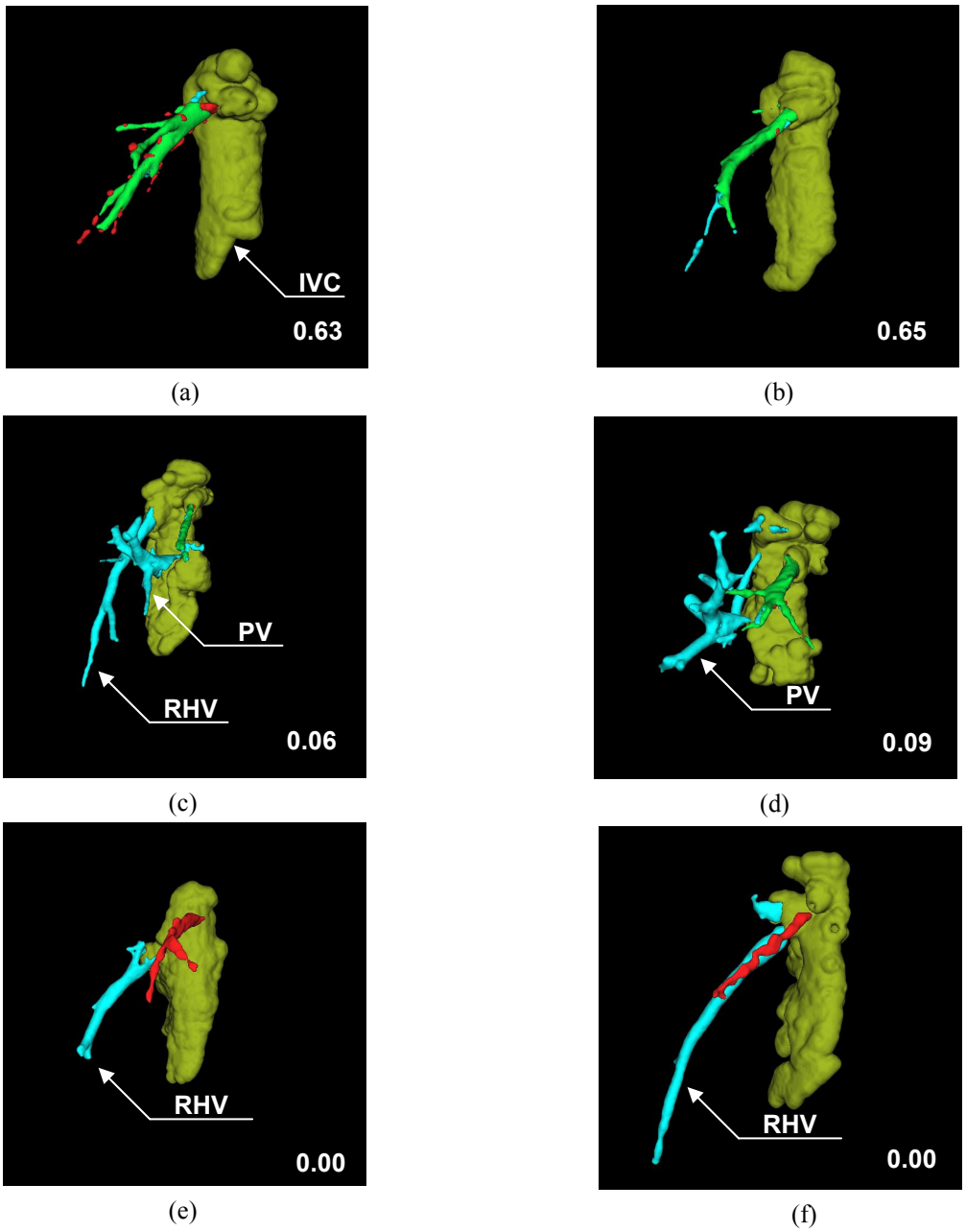

Fig.9 Results of extracted MHV regions (two cases each. green: overlapping region, blue: over extraction, red: under extraction.) Coincidence ratios are indicated in lower right hand corners. (a) & (b) successful results, (c) & (d) unsuccessful results (over extraction of RHV: right hepatic vein, PV: portal vein), and (e) & (f) unsuccessful results (RHV extraction).

regions (PV, right liver vessel: RHV). Figs.9 (e) and (f) also indicate unsuccessful cases in non-MHV regions (RHV) are extracted.

The location of MHV region could be identified successfully by our purposed method. However, the accuracy of the shape of the MHV in the extracted results was not good enough. This problem may be caused by the poor accuracy of the atlases and should be resolved by adding more CT cases as learning samples during the atlas construction.

5. CONCLUSION

We proposed an automated method to segment MHV in non-contrast X-ray CT images based on an atlas-driven approach. The efficiency of the method was confirmed using 22 normal liver cases. It was found that the mean value of coincidence ratios between the extracted MHV and corresponding gold standard in each CT case was 0.374, thus and the effectiveness of our MHV extraction method was shown.

ACKNOWLEDGMENTS

This research was supported in part by Grant-in-Aid for Scientific Research from the Ministry of Education, Culture, Sports, Science, and Technology (MEXT), Japanese Government.

REFERENCES

1. D. Selle, B. Prem, A. Schenk, and H.-O. Peitgen, "Analysis of vasculature for liver surgical planning," IEEE Trans. on Med. Imag., vol.21, pp.1344-1357, 2002.
2. B. B. Frericks, F. C. Caldarone, B. Nashan, D. H. Savellano, G. Stamm, T. D. Kirchhoff, H. –O. Shin, A. Schenk, D. Selle, W. Spindler, J. Klempnauer, H.-O. Peitgen, and M. Galanski, "3D CT modeling of hepatic vessel architecture and volume calculation in living donated liver transplantation," Eur. Radiol., vol.14, pp.326-333, 2004.
3. H. Kobatake, A. Shimizu, X. Hu, L.-L. Huang, Y. Hagihara, and S. Nawano, "Simultaneous segmentation of multiple organs in multi-dimensional medical images", in Symposium on Future CAD, Proc. of The First International Symposium on Intelligent Assistance in Diagnosis of Multi-Dimensional Medical Images, pp. I-11-28, 2005.
4. S. Tamura, Y. Sato, Y. Nakajima, T. Johkoh, N. Sugano, and M. Hori, "Computational modeling of organ structures," in Symposium on Future CAD, Proc. of The First International Symposium on Intelligent Assistance in Diagnosis of Multi-Dimensional Medical Images, pp. I-19-24, 2005.
5. Y. Sato, T. Okada, M. Nakamoto, Y. W. Chen, M. Hori, N. Sugano, and S. Tamura, "Computational modeling of anatomical structures," in Symposium on Future CAD, Proc. of The First International Symposium on Intelligent Assistance in Diagnosis of Multi-Dimensional Medical Images, pp.42-49, 2006.
6. A. Shimizu, R. Ohono, T. Ikegami, H. Kobatake, S. Nawano, and D. Smutek, "Simultaneous extraction of multiple organs from abdominal CT," in Symposium on Future CAD, Proc. of The First International Symposium on Intelligent Assistance in Diagnosis of Multi-Dimensional Medical Images, pp.42-49, 2005.
7. S. Kawajiri, X. Zhou, X. Zhang, T. Hara, H. Fujita, R. Yokoyama, H. Kondo, M. Kanematsu, and H. Hoshi, "Automated segmentation of hepatic vessel trees in non-contrast X-ray CT images," Proc. of SPIE, vol.6512, 65123A-1-65123A-8, 2007.
8. T. Kitagawa, X. Zhou, T. Hara, H. Fujita, R. Yokoyama, M. Kanematsu, and H. Hoshi, "A probabilistic atlas generation method for liver region using non-contrast torso CT images," The program of 91st Scientific Assembly and Annual Meeting of the RSNA, p. 856, 2005.
9. X. Zhou, T. Kitagawa, T. Hara, H. Fujita, X. Zhang, R. Yokoyama, H. Kondo, M. Kanematsu, and H. Hoshi, "Constructing a probabilistic model for automated liver region segmentation using non-contrast X-ray torso CT images," Proc. of 9th International Conference for MICCAI 2006, Part II, vol.4191, pp.856-863, Springer Berlin/Heidelberg, 2006.
10. T. Kitagawa, X. Zhou, T. Hara, H. Fujita, R. Yokoyama, H. Kondo, M. Kanematsu, and H. Hoshi, "Liver atlas construction and evaluation using non-contrast torso CT images," International Journal of Computer Assisted Radiology and Surgery, vol.1, sup.1, p.524, 2006.

11. X. Zhou, T. Hara, H. Fujita, R. Yokoyama, H. Cheng, T. Kiryu, and H. Hoshi, “Automated estimation of the upper surface of the diaphragm in 3-D CT images”, IEEE Trans. Biomed. Eng., vol.55, no.1, pp.351-353, 2008.
12. X. Zhou, T. Hara, H. Fujita, R. Yokoyama, T. Kiryu, M. Kanematsu, and H. Hoshi “Preliminary study for automated recognition of anatomical structure from torso CT images”, Proc. of the 2005 IEEE Engineering in Medicine and Biology 27th Annual Conference, pp.650-653, 2005.
13. F. L. Bookstein, “Principal warps: Thin-plate splines and the decomposition of deformations”, IEEE Trans. Pat. Anal. Mach. Intell., vol.11, no.6, pp.567-585, 1989.
14. Y. Sato, S. Nakajima, H. Atumi, S. Yoshida, T.Koller, G. Gerig, and R. Kikinis, “Three-dimensional multi-scale line filter for segmentation and visualization of curvilinear structures in medical images”, Medical Image Analysis, vol.2, no.2, pp.143-168, 1998.